International Journal of Architectural, Civil and Construction Sciences
ISSN: 2415-1734
Vol:5, No:12, 2011

Determination of Stress-Strain Characteristics of Railhead Steel using Image Analysis

Bandula-Heva, T., Dhanasekar, M.

***Abstract*—**True stress-strain curve of railhead steel is required to investigate the behaviour of railhead under wheel loading through elasto-plastic Finite Element (FE) analysis. To reduce the rate of wear, the railhead material is hardened through annealing and quenching. The Australian standard rail sections are not fully hardened and hence suffer from non-uniform distribution of the material property; usage of average properties in the FE modelling can potentially induce error in the predicted plastic strains. Coupons obtained at varying depths of the railhead were, therefore, tested under axial tension and the strains were measured using strain gauges as well as an image analysis technique, known as the Particle Image Velocimetry (PIV). The head hardened steel exhibit existence of three distinct zones of yield strength; the yield strength as the ratio of the average yield strength provided in the standard (σ_{yr}=780MPa) and the corresponding depth as the ratio of the head hardened zone along the axis of symmetry are as follows: (1.17 σ_{yr}, 20%), (1.06 σ_{yr}, 20%-80%) and (0.71 σ_{yr}, > 80%). The stress-strain curves exhibit limited plastic zone with fracture occurring at strain less than 0.1.

***Keywords*—**Stress-Strain Curve, Tensile Test, Particle Image Velocimetry, Railhead Metal Properties

I. Introduction

RAIL modelling using finite element (FE) is one of the widely used solution techniques for uncovering numerous rail related problems. The accuracy of the FE solution technique depends on the appropriateness of the input material properties. In addition to the elastic material properties (Young's modulus and Poison's ratio), a complete true stress-strain curve of rail steel is required to perform accurate plastic analysis. With a view to improving wear resistance [1, 2], railheads are often case hardened using heat treatment. The head hardened rails are used in most heavy haul corridors[3] around the world owing to their superior fatigue and wear resistance. Although technologies are available to fully hardened the whole of the railhead (or the entire rail in some instances), owing to economy, partly head hardened rails are used in Australia; in such railheads the hardening is not performed uniformly across the railhead. In such cases a unique stress-strain curve cannot be representative for the whole of the railhead metal. AS1085.1-Fig.F1[4] defines the enclosed area ABCDEF of Fig. 1 as the heat affected zone, where the rail steel is deemed to be harder.

Uniaxial monotonic tensile test of strain gauged coupons is the easiest and well known method to determine the stress-strain characteristics of metals.

S.Rajanna et al.[5] conducted tensile test to explore the stress-strain characteristics of heat treated thermite welded rail steel.

Bandula Heva, T. Faculty of Built Environment and Engineering, Queensland University of Technology, Australia.

Dhanasekar, M. Faculty of Built Environment and Engineering, S-714, Gardens Point Campus, Queensland University of Technology, Brisbane QLD 4000 Australia. (phone: +61-7-3138-6666; fax: +61-7-3138-1170; e-mail: m.dhanasekar@qut.edu.au).

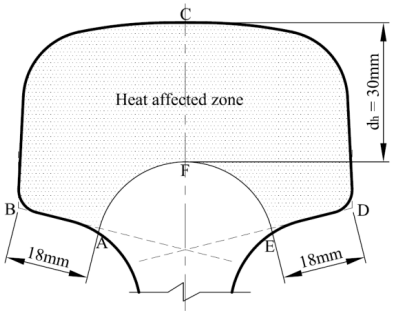

Fig. 1 Heat affected zone of AS60 railhead

Some examples of tensile tests of steel with strain gauge application are reported in the papers published by Anapayan et al.[6], Qin et al.[7] and Rivera et al.[8]. Unfortunately in most tests it is noted that after a critical strain level (approximately 200,000 microstrain), strain gauges tend to delaminate; therefore, it is widely regarded that the strain gauges are not appropriate for recording very high levels of strains. To obtain full stress-strain curves Hoffmann and Vogl[9] used an expensive optical system, known as "Gesellschaft fur Optische Messtechnik mbH [10] (in German)" to measure strains in coupons under monotonic tensile load. Recently, Yang et al.[11] reported the application of Digital Image Correlation, (DIC) technique with a sophisticated high speed camera to obtain the stress-strain curve of steel. To the best of the knowledge of the authors, railhead material properties of head hardened rail are not available in the open literature; therefore, it was decided to test the railhead material for nonlinear properties. A set of 10 coupons sampled from varying depths of the railheads were tested under axial tension for this purpose. In addition to strain gauges, an image analysis technique, known as Particle Image Velocimetry (PIV), was used for measuring the strains. With the PIV method it was possible to measure the lateral strains in addition to the axial strains of the test coupons. Strains measured using strain gauges was used to validate the PIV data. The lateral strain obtained from the PIV was used to determine the true cross sectional area of the test coupons and hence the true stress.

II. Particle Image Velocimetry (PIV)

PIV was originally developed to measure velocity of particles in the experimental fluid mechanics as narrated in the measurement of local velocity of a seeded flow by Adrian[12]. More details of the PIV are explained in Raffel et. al[13]. The PIV technique was modified by White and Take[14] for the geotechnical testing. In the modified technique, they replace the seeding in the fluid with texture of natural sand particle of the exposed surface of soil. They also proposed to add texture by adding colored 'flock' or dyed sand on the exposed plane. In 2002, they developed a Matlab module[15] known as GeoPIV for analyzing digital images in the PIV. In the PIV

operation, the texture of an image is tracked through a series of images. The movements (displacements) of the visible surface of the soil particles are determined. A perfectly stationary camera is essential to capture the motion of the particles throughout the period of testing as any minor movement of the camera can affect the accuracy of the results significantly.

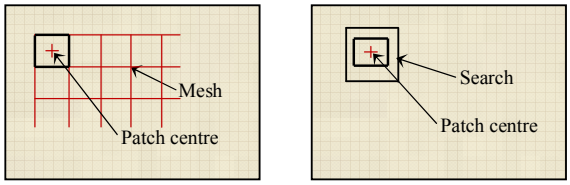

Fig. 2 Principles of PIV analysis[15]

For the PIV, a series of photos of the zone of interest is taken starting from the unloaded stage; the photos in the loaded stage are compared to the initial photo corresponding to the unloaded stage to analyse tracing of the particle movement. Firstly, the interested area of the first digital image is divided into a mesh of cells (or, patches) as shown in Fig. 2. The size of a patch and the distance between patches can be decided according to research requirements. The centroidal coordinates (u_1,v_1) of the colored texture of each patch of Image 1 is tracked within the search patch area of Image 2 (u_2,v_2). The size of the search patch area is set according to the research requirements. If the search patch size is very large, the tracking time will be longer, which will make the process uneconomical and cumbersome. Finally a set of coordinates of the patch centre locations for each of the successive images is generated. The patch coordinate data are used to evaluate the relative movements of the particles.White et al.[14, 16] successfully applied the PIV image analysis technique to measure the deformation of soil under load. They took images for the PIV analysis using a 2-megapixel digital camera. Thusyanthan et al.[17] used PIV image analysis technique to measure strain of a clay beam.In this research, PIV was used to measure steel strains for the first time to the best of the author's knowledge. As steel does not have contrasting color/ texture similar to soil, the steel surface was dotted with color marker pens.

III. Experiment

A. Test coupon preparation

Tensile test coupons were prepared as per the provisions in Australian standard AS1391[18]; the dimensions of a typical coupon is as shown in Fig. 3.

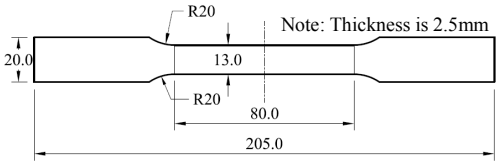

Fig. 3 Dimensions of rail test coupon

Seven samples (A1 to A7) were obtained from a railhead as shown in Fig. 4. Since the top of the railhead is usually subjected to severe levels of wheel loading, additional three specimens (B1 to B3) were sampled from another Rail (B). Both rails (A and B) were virgin.

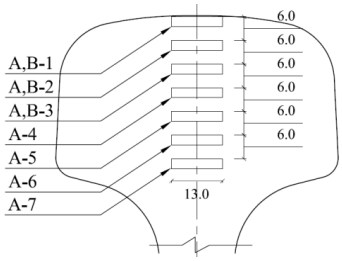

Fig. 4 The locations of the test coupons in railhead.

As heat can significantly change the properties of rail steel, extreme care was taken to control the temperature of the samples closer to ambient during cutting, grinding and polishing operations of the rail test coupons. A strain gauge was attached on one flat side of each test coupon. Black and red color marker pens were used to dot the non-strain gauges side of the test coupons as shown in Fig. 5(a) for facilitating PIV analysis.

B. Experimental procedure

The coupons were tested in an INSTRON tensile testing machine of 50kN capacity. The tensile testing setup is as shown in Fig. 5(b). The coupons were tested under monotonic tension under the displacement control mode with low elongation rate (1mm/minute) to justify the static loading requirements. The digital images of the dotted surface of test coupons were taken, during the testing, at a rate of one image per each four seconds (0.25Hz) using a canon EOS 450D digital camera. The time load history from tensile testing machine, digital images and strain gauge readings were obtained for all the ten rail test coupons as the test outputs.

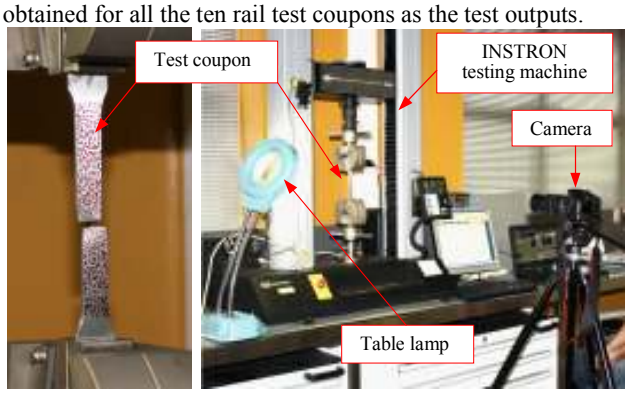

Fig. 5 (a) Colored marker pen dots on coupon surface, (b) Tensile testing setup

IV. Data Analysis

A. Determination of strain with PIV

The PIV image analysis software produced a "txt" file for each image which contained the patch centre coordinates. The distance between two patches of the first image (l_0) can be determined based on the PIV output. The distance between the

same two patches of the series of other images (l_1, l_2, l_3, ...l_t) can also be determined from the successive images. Then the strain (ε_t) at a given time t is determined as follows:

$$\varepsilon_t = \frac{l_t - l_0}{l_0} \quad (1)$$

B. Determination the Parameters of Stress-Strain Curve

Key features of a typical engineering and true stress-strain curves for metal are described by the curves OABCDE and OABCE` respectively as shown in Fig. 6. For establishing the engineering stress-strain curve, the stresses were determined using the original cross sectional area of the test coupon, whereas for the true stress-strain curve, the stress was determined using the progressively diminishing area of cross section. The slope of the initial linear part of tensile test curve is taken as the Young's modulus. Ductile materials show considerable perfect plastic region (curve BC); a perfect plastic region cannot be seen for brittle materials. It is difficult to identify exact yield point in most situations. Therefore a straight line was drawn parallel to the initial linear part of the curve so that the line cuts the strain axis at 0.002(proof strain) as shown in Fig. 7. The intersection point of this line and stress-strain curve is known as yield point and the corresponding stress is referred as yield stress or 0.2% yield strength.

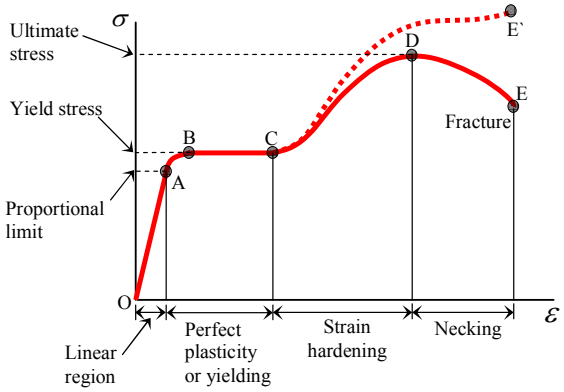

Fig. 6 Typical stress-strain curve of metals[19]

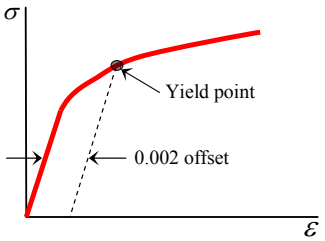

Fig. 7 Offset line through 0.002 strain to obtain Yield point

The test coupons elongates axially during the tensile test which consequently lead to reduction in its cross sectional area. Since the determination of lateral strain is possible with PIV image analysis during the tensile test (especially for large strain range), a relationship between the lateral strain and the cross sectional area can be developed as described in this section.

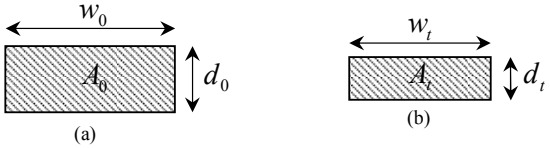

Fig. 8 (a) Initial cross sectional area, (b) Cross sectional area at time t

Eq. (2) and Eq. (3) describe the reduction in cross section over the time t.

$$w_t = w_0(1-\varepsilon_{tw}) \quad (2)$$

$$d_t = d_0(1-\varepsilon_{td}) \quad (3)$$

where, w_0, d_0, w_t and d_t are cross sectional dimension of test coupon at initially and at time t as shown in Fig. 8. The corresponding cross sectional areas are A_0 and A_t respectively. The strain in the direction of width and thickness at time t are ε_{tw} and ε_{td} respectively.

Multiplying Eq. (2) with Eq. (3);

$$w_t d_t = w_0 d_0 (1-\varepsilon_{tw})(1-\varepsilon_{td}) \quad (4)$$

Since $w_t d_t = A_t$ and $w_0 d_0 = A_0$;

$$A_t = A_0(1-\varepsilon_{tw})(1-\varepsilon_{td}) \quad (5)$$

Considering the isotropic hypothesis for rail steel;

$$\varepsilon_{tw} = \varepsilon_{td} = \varepsilon_t \quad (6)$$

where, ε_t is the lateral strain at time t.

Then from Eq. (5) and Eq. (6);

$$A_t = A_0(1-\varepsilon_t)^2 \quad (7)$$

Since the lateral strain is known, the corresponding cross sectional area for a particular time can be determined using the Eq. (7). Then the engineering stress ($\sigma_{t,ENG}$) and true stress ($\sigma_{t,TRUE}$) at time t is given by the Eq. (8) and Eq. (9) respectively.

$$\sigma_{t,ENG} = \frac{F_t}{A_0} \quad (8)$$

$$\sigma_{t,TRUE} = \frac{F_t}{A_t} \quad (9)$$

where, F_t is the axial load on test coupon at time t.

C. Validation of PIV strain

Since the application of PIV method to steel strain determination is new, it has been decided to validate the steel strains from the PIV method using the engineering stress-strain curve for rail steel determined from the strain gauge data. The engineering stress-strain curves of a typical test specimen obtained from the PIV method and from the strain gauge data are shown in Fig. 9. The true stress-strain curve is

also included in the same figure. Even though the strain gauges produced accurate strains during the initial part of the tensile test, strain gauges de-bonded before reaching 0.03 strains. Thus a full stress-strain curve based on strain gauge readings cannot be seen in Fig. 9. However, there is a good agreement between engineering stress-strain curve from PIV method and from strain gauge readings can be seen in the initial part of the plot as shown in Fig. 9.

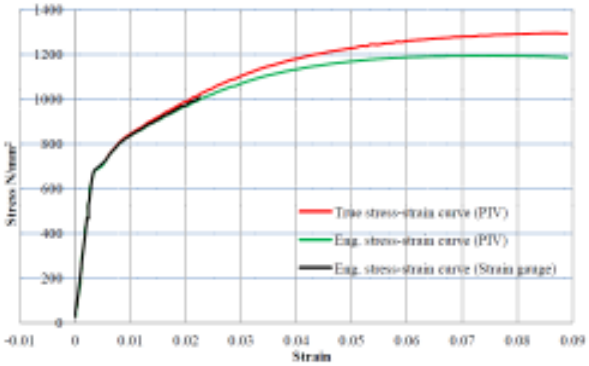

Fig. 9 Stress-strain curves for a rail test coupon (A4)

D.Result discussion

The true stress-strain curves and engineering stress-strain curves for all ten test coupons are shown in Fig. 11 and Fig. 12 respectively. According to these plots, the rail steel does not show significant perfect plasticity region. A necking phenomenon also cannot be seen in any of the engineering stress-strain curves in Fig. 12. The head hardened rail steel is therefore regarded less ductile compared to other common steels. The broken tensile test coupons justified the low ductile characteristics of rail steel as shown in Fig. 10. Generally the surfaces fractured prior to necking.

Fig. 10 Broken rail test coupons after tensile test

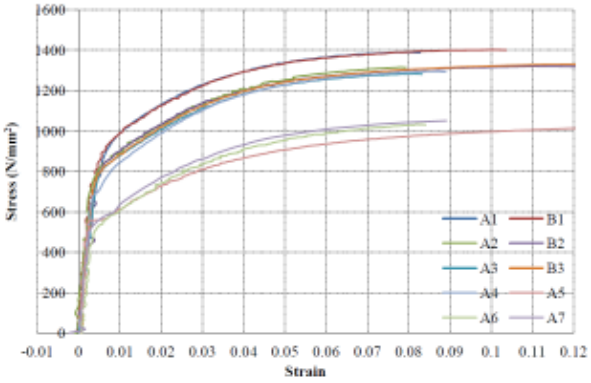

Fig. 11 True stress-strain curves for all test coupons

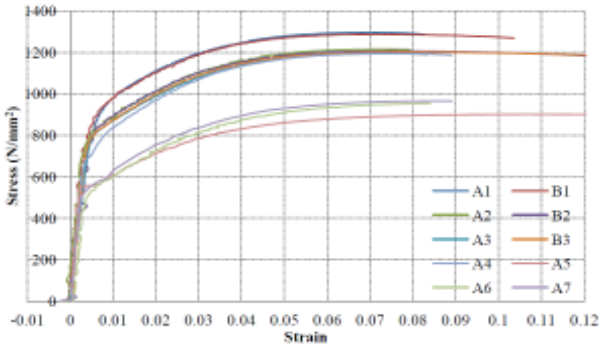

Fig. 12 Engineering stress-strain curves for all test coupons

Confirming the accuracy of the experiment, the test coupons obtained from the same depth from rail A and rail B show very good agreement of the stress-strain characteristics and 0.2% yield strength as shown Fig. 11, Fig. 12 and Fig. 13. According to these figures, the test coupon A1 and B1 show highest tension capacity. The test coupon A2, B2, A3, B3 and A4 show inter mediate tension capacity and the test coupon A5, A6 and A7 show lowest tension capacity. Thus, three different material property zones can be identified in railhead.The Young's modulus and 0.2% Yield strength of rail steel are specified in Australian standard[4] as (E_r=) 207GPa and (σ_{yr}=) 780MPa respectively. The Young's modulus (E) and 0.2% Yield strength (σ_y) obtained from the rail test specimens as ratios of the values specified in the Australian standard[4] are tabulated in the Table I. In this table, the maximum engineering strength (σ_{ENG}) and the maximum true strength (σ_{TRUE}) of test coupons are also non-dimensionalised based on the 0.2% Yield strength provided in the standard. The variation of the 0.2% Yield strength ratio against depth ratio is as shown in Fig. 13.

TABLE I
SUMMARY OF THE MATERIAL PARAMETERS OBTAINED FROM TENSILE TEST

Test Coupon	Young's Modulus Ratio (E / E_r)	0.2% Yield Strength Ratio (σ_y / σ_{yr})	Max Eng. Stress Ratio (σ_{ENG} / σ_{yr})	Max True Stress Ratio (σ_{TRUE} / σ_{yr})
B1	1.002	1.168	1.650	1.795
B2	0.998	1.083	1.546	1.692
B3	1.015	1.038	1.541	1.705
A1	0.974	1.163	1.663	1.781
A2	1.019	1.077	1.558	1.687
A3	0.947	1.046	1.531	1.645
A4	1.024	0.929	1.531	1.660
A5	1.010	0.719	1.156	1.301
A6	0.980	0.690	1.223	1.324
A7	1.005	0.712	1.237	1.347

The Young's modulus obtained from the test coupons are well agreed with the value specified in the Australian standard[4]. The location of test coupon to be cut from rail head for tensile testing is specified in the same standard. Since the locations of the test coupons obtained from railhead in this experiment are different from the location specified in the standard, the comparison of tensile strength and 0.2% yield strength obtained from this experiment with those mentioned in the standard is not appropriate. However, the Australian standard gives conservative tensile strength and 0.2% yield strength compared to this experiment result shown in table I.

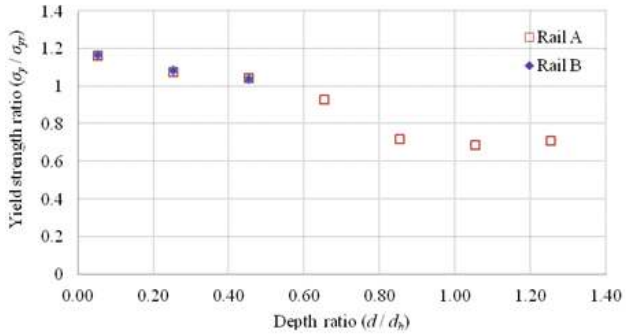

Fig. 13 Variation of rail head 0.2% Yield strength ratio against depth ratio (depth d / heat affected zone depth d_h)

V. Conclusion

In this paper, the stress-strain characteristics of the railhead and their variations within the depth of the railhead are presented. The stress-strain data were determined from tensile testing of coupons conforming to the dimensions listed in AS1391[18], which are cut out from the railhead. The testing of coupons was carried out in an INSTRON machine that applied the tensile load whilst the deformation of the coupons was determined using a digital image analysis technique known as the Particle Image Velocimetry (PIV).

The following conclusions are obtained:

- The PIV image analysis technique can be successfully used to measure metal strains. Since the PIV image analysis method needs only a series of digital images, it can be a cheap means of measuring strains compared to other optical strain measuring techniques that needs high speed camera or sophisticated computer programs with laser guns.
- The rail steel show limited plastic strain in the hardening region with the associated brittle fracture; necking typical of steel failure under tension was not visible. Most of the railhead test coupons broke at about 0.1 strains.
- The head hardening treatment is not uniformly distributed within the heat affected zone. It appears there exist three distinct zones within the railhead. Based on the experiment results, top metal layer of railhead up to approximately 20% depth of the heat affected zone shows highest tensile yield strength of approximately $1.17\sigma_{yr}$. The depth from about 20% to 80% shows intermediate tensile yield strength approximately $1.06\sigma_{yr}$ and the depth below 80% shows lowest tensile yield strength in the order of only $0.71\sigma_{yr}$.

Acknowledgements

The financial support of the Cooperative Research Centre for Rail Innovation is acknowledged with thanks. The involvement of Ciaran Byrne and Bence Sipos, Engineering students of the Queensland University of Technology is thankfully acknowledged. The workshop and the material testing laboratory staff of the Queensland University of Technology assisted at many stages of the project.

References

[1] X. Zhan. and S. Wang, "Research on the improvement of Rail head hardening technology on Railway," *Journal of the Eastern Asia Society for Transportation Studies,* vol. 5, pp. 263-271, 2005.
[2] D.F. Cannon and H. Pradier, "Rail rolling contact fatigue research by the European Rail Research Institute," *Wear,* vol. 191, pp. 1-13, 1996.
[3] A.K. Hellier and A.A. Merati, "The mode I fatigue threshold for head hardened rail steel," *International Journal of Fatigue,* vol. 20, pp. 247-249, 1998.
[4] AS 1085.1., Standards-Australia., " Railway track materials, Part 1: Steel rails," *Australian Standard,* 2002.
[5] S. Rajanna, H.K. Shivanand, and B.N. Akash Deep, "Improvement in mechanical behavior of expulsion with heat treated thermite welded rail steel," *Proceedings of World Academy of Science, Engineering and Technology,* vol. 60, pp. 558-562, 2009.
[6] T. Anapayan, M. Mahendran, and D. Mahaarachchi, "Lateral distortional buckling tests of a new hollow flange channel beam," *Thin-Walled Structures,* vol. 49, pp. 13-25, 2011.
[7] M. Qin, V. Ji, Y.N. Wu, C.R. Chen, and J.B. Li, "Determination of proof stress and strain-hardening exponent for thin film with biaxial residual stresses by in-situ XRD stress analysis combined with tensile test," *Surface and Coatings Technology,* vol. 192, pp. 139-144, 2005.
[8] E. Rivera, D.J. Thomson, and A.A. Mufti, "Comparison of recoated fiber Bragg grating sensors under tension on a steel coupon," in *Nondestructive Evaluation and Health Monitoring of Aerospace Materials, Composites, and Civil Infrastructure IV*, 2005, pp. 163-174.
[9] H. Hoffmann and C. Vogl, "Determination of True Stress-Strain-Curves and Normal Anisotropy in Tensile Tests with Optical Strain Measurement," *CIRP Annals - Manufacturing Technology,* vol. 52, pp. 217-220, 2003.
[10] K. Ichinose, K. Fukuda, K. Gomi, K. Taniuchi, and M. Sano, "Yield strength in relation to cyclic loading," *Journal of Testing and Evaluation,* vol. 29, pp. 529-34, 2001.
[11] Y. Lianxiang, S. Lorenzo, G. Abhishek, and C. Xu, "Measure Strain Distribution Using Digital Image Correlation (DIC) for Tensile Tests," The Advanced High Strength Steel Stamping Team of the Auto/Steel Partnership (A/SP) 2010.
[12] R.J. Adrian, "Particle-Imaging Techniques for Experimental Fluid Mechanics," *Annual Review of Fluid Mechanics,* vol. 23, pp. 261-304, 1991.
[13] M. Raffel, C.E. Willert, S.T. Wereley, and J. Kompenhans, "Particle Image Velocimetry : A Practical Guide," Springer, 2007.
[14] D.J. White, W.A. Take, and M.D. Bolton, "Soil deformation measurement using particle image velocimetry (PIV) and photogrammetry," *Geotechnique,* vol. 53, pp. 619-631, 2003.
[15] D.J. White and W.A. Take, "GeoPIV: particle image velocimetry (PIV) software for use in geotechnical testing (Technical Report)," Cambridge University Department of Engineering 2002.
[16] D.J. White, W.A. Take, and M.D. Bolton, "Measuring soil deformation in geotechnical models using digital images and PIV analysis," in *10th International Conference on Computer Methods and Advances in Geomechanics. Tucson, Arizona.*, 2001, pp. 997-1002.
[17] N.I. Thusyanthan, W.A. Take, S.P. Madabhushi, and M.D. Bolton, "Crack initiation in clay observed in beam bending," *Geotechnique,* vol. 57, pp. 581-594, 2007.
[18] AS1391., Standard-Australia., "Metallic materials-Tensile testing at ambient temperature," *Australian Standard,* 2007.
[19] J.M. Gere. and B.J. Goodno., "Stress-Strain Diagrams," in *Mechanics of materials* 7th ed: Cengage Learning, 2009, p. 19.